Korean J. Chem. Eng., 39(12), 3295-3304 (2022)
DOI: 10.1007/s11814-022-1209-x

pISSN: 0256-1115
eISSN: 1975-7220

Cell performance and polarization analysis on different operating conditions in anion exchange membrane-unitized regenerative fuel cells (AEM-URFCs)

Md. Masud Rana*, Gyungse Park, Ho-Jung Sun***, Hyung-Ryul Rim****, Hong-Ki Lee****, and Joongpyo Shim*,†**

*Department of Chemical Engineering, Kunsan National University, Jeonbuk 54150, Korea
**Department of Chemistry, Kunsan National University, Jeonbuk 54150, Korea
***Department of Material Science and Engineering, Kunsan National University, Jeonbuk 54150, Korea
****Fuel Cell Regional Innovation Center, Woosuk University, Jeonbuk 55315, Korea
(*Received 17 February 2022 • Revised 9 May 2022 • Accepted 16 June 2022*)

Abstract−Several electrode parameters and operating conditions were investigated on the cell performance of anion exchange membrane-unitized regenerative fuel cell (AEM-URFC). The AEM-URFC's performance increased with increasing the ionomer and catalyst contents on the electrode up to an optimum amount and then decreased due to the blockage of mesopores on the catalyst layers. The AEM-URFC with optimal ionomer and catalyst loaded showed the maximum current (255.0 mA/cm^2) and power (127.5 mW/cm^2) density at 0.50 V for fuel cell mode at 60 °C. Also, three different kinds of commercial AEMs were tested in URFC. The catalyst for the bifunctional oxygen electrode had a pronounced influence on the cell performance of AEM-URFC. Ir black showed the highest WE performance than other precious catalysts (Pt/C, PtRu black, and IrO_2), but lower performance in FC mode than Pt/C and PtRu catalysts. The optimized AEM-URFC had 48.30% round trip efficiency, which is comparable or superior to the results reported in the literature.

Keywords: Anion Exchange Membrane, Unitized Regenerative Fuel Cells, Ionomer Content, Catalyst Loading, PtRu Catalyst, Iridium Black

INTRODUCTION

The use of fossil fuels for energy production daily exceeds the tolerable level of global warming. Therefore, the demand for sustainable and environmentally friendly energy sources increases in today's world [1]. Recently, energy storage and conversion by electrochemical cells, such as rechargeable and flow batteries, fuel cells, and super-capacitors, have been hot issues for storing energy. Regenerative fuel cell (RFC) is at the front of the selection race. A regenerative fuel cell, one of the fuel cell types, is a promising energy conversion system from hydrogen and oxygen to electricity, and vice versa. The RFC system has two units, a water electrolyzer (WE) and a fuel cell (FC). FC is a unit for producing electricity using hydrogen and oxygen and, conversely, a WE is a unit for producing hydrogen and oxygen using electricity. This RFC system has distinctive advantages over rechargeable batteries with its long-term energy storage and high specific energy [2,3]. However, applications of the RFC system have been limited because of the high cost and complexity of these systems. To resolve these problems, unitized regenerative fuel cells (URFC) have been developed in an integrated single unit including a fuel cell and a water electrolyzer. Proton exchange membrane-based URFC (PEM-URFC) has been studied since the early 1990s [4]. Nafion and platinum group metals (PGM) are used as PEM and catalysts because of their high ionic conductivity and better catalytic activity, respectively [5,6]. However, PEM-URFC still has limitations because of the high cost of catalyst materials. Anion exchange membrane (AEM) is hydroxyl ions (OH^- ions) conducting polymer, which is one of the key components in AEMFC (Anion exchange membrane fuel cell) or AEMWE (Anion exchange membrane water electrolyzer), and should have high ionic conductivity, ultimately low gas permeability, non-electric conductivity, and chemical stability [7-9]. Recently, commercially available AEM, such as Tokuyama and Fumatech, were used for AEMFCs [10,11].

Although the research for AEMFC or AEMWE has been conducted independently by many scientists, AEM-URFC has barely been studied. In this study, the AEM-URFC performance in FC and WE modes was investigated on the electrode and operation parameters, such as ionomer content, water feeding modes, catalyst loading, different membrane types, cell temperature, and bi-functional oxygen electrode catalysts, to provide basic data for the researchers concerned. The AEM-URFCs were fabricated with Fumasep FAA-3 series as AEMs, which are the commercial product of Fumatech GmbH, and noble metal catalysts.

EXPERIMENTAL

For AEM-URFC fabrication, commercial catalyst Pt/C (40 wt%, Alfa Aesar) was chosen as a bi-functional hydrogen electrode (BHE) catalyst and bi-functional oxygen electrode (BOE), with different catalysts such as PtRu/C (60 wt%, 1 : 1 atomic ratio, Alfa Aesar),

†To whom correspondence should be addressed.
E-mail: jpshim@kunsan.ac.kr

PtRu-black (PtRu-B), Ir-black (Ir-B), and IrO_2 (Premetek. Co), were used. We used a commercial anion exchange membrane (Fumasep FAA-3, Fumatech GmbH) and ionomer (Fumion FAA-3-SOLOUT-10, 10 wt%, Fumatech GmbH). The other chemicals, such as KOH (SHAMCHUN) and isopropyl alcohol (IPA, SHAMCHUN), were laboratory grade.

The membrane electrode assembly (MEA) for AEM-URFC was fabricated by the catalyst-coated membrane (CCM) method, which might successfully diminish the ionic resistance between the catalyst layer and AEM [12]. The BHE catalyst ink was prepared by a commercial Pt/C catalyst and ionomer ultrasonically mixed with 2 ml deionized (DI) water and 3 ml IPA for 10 minutes. The ratio of water to IPA was 2 : 3. The as-prepared catalyst inks were directly sprayed from a spray gun on the surface of a commercial anion exchange membrane (AEM) by placing them on the hot plate at 60 °C. Pure N_2 (99.9%) gas was used in the spray gun for the ink painting (Fig. 2(a)). The active surface area of the catalyst layer was 4 cm^2. Similarly, the BOE was prepared the same as the BHE electrode. For complete anion exchange of the membrane (bromide form to hydroxyl form), the fabricated CCM has immersed in 1.0 M KOH solution for 24 h. To remove the KOH from the CCM surface, it was washed thoroughly with DI water several times. Then membrane electrode assembly (MEA) was fabricated by placing gas diffusion layers, carbon paper (Av-Carb 1120, Ballard) for BHE, and Ni foam (1.6 mm thick, MTI) for BOE on both sides of the CCM. Immediately, the fabricated MEA was placed between graphite (BHE side) and nickel (BOE side) plates having a gas channel of 1.0 mm wide and 1.0 mm depth. Two silicone gaskets were placed on both sides of the MEA and clamped with the screw by applying a 30 kg/cm^2 force (Fig. 2(b)).

The AEM-URFC's performance was evaluated by a single cell with an active area of 4 cm^2 in dual fuel cell (FC) and water electrolysis (WE) modes. In FC mode, the AEM-URFCs operate at 50-70 °C and atmospheric pressure. The reactant gases, pure hydrogen (100 ccm/min) (99.99%), and oxygen (200 ccm/min) (99.99%) were humidified to 100% relative humidity in the water bath and directly fed to the BHE and BOE sides, respectively. In the WE mode, ultra-pure deionized water (DI water) at 50-70 °C was supplied to the electrode from a water reservoir (Fig. 2(c)). The water feeding rate was 2.25 ml/min for all water feeding modes (BHE/BOE or both modes). Different ionomer content and catalyst loading effects on the AEM-URFCs performances were evaluated. In FC and WE modes after proper activation, the current density was recorded from the open-circuit voltage (OCV) to the certain voltage (0.3 V) by stepping of 100 mV voltage controlled by electronic load (DAE GIL) and a power supply (MK Power). The round-trip (RT) efficiencies were calculated by using the following equation:

$$RT = \frac{V_{FC}}{V_{WE}}$$

where V_{FC} and V_{WE} are the cell potential at a specific current density.

The potential difference (ΔV) between two modes (FC & WE) was calculated by subtracting the output cell potential (FC potential) from input cell potential (WE potential) at a specific current density.

$$\Delta V = V_2 - V_1$$

where V_2 is the cell potential in WE mode and V_1 is the cell potential in FC mode at a specific current density.

1. Characterization

The catalyst surface morphology and layer thickness of the prepared CCMs was observed by the ultra-high-field emission scanning electron microscope (Ultra-High FE-SEM, HITACHI, SU8280) with an accelerated voltage of 3.0 KV. The electrochemical impedance spectra (EIS) of the fabricated MEAs were evaluated by the EIS spectrometer (ZIVE SP1) with a frequency range of 0.1 Hz to 1 MHz.

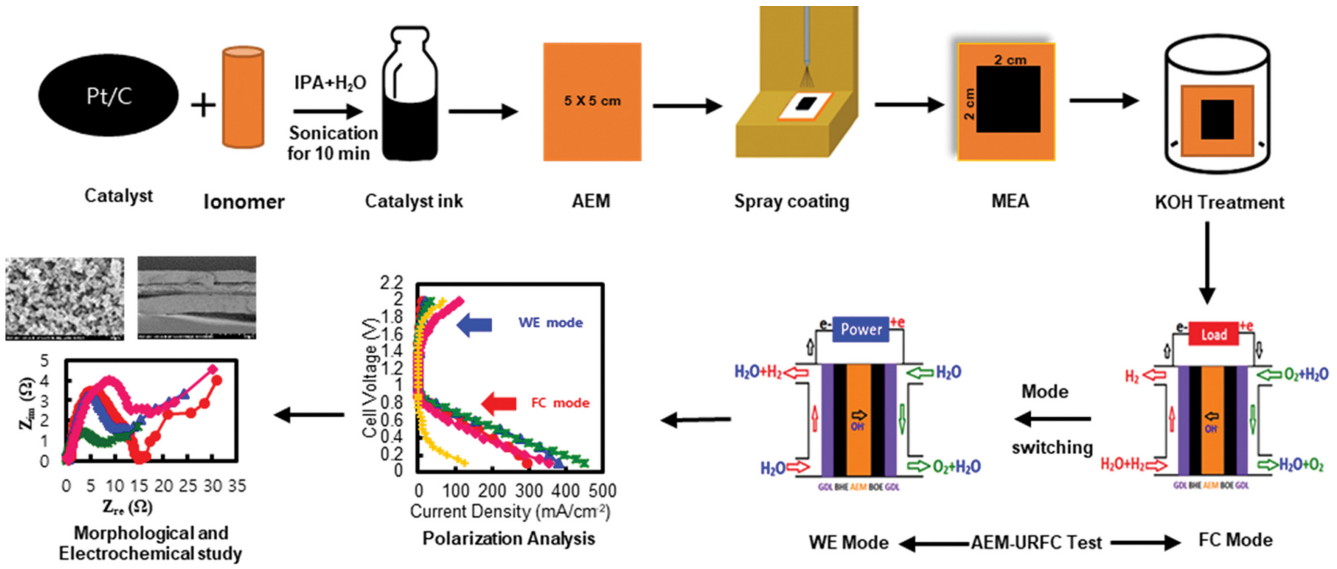

Fig. 1. Schematic illustration of the cell performance and polarization analysis of AEM-URFC fabricated with commercial membranes, catalysts, and ionomer.

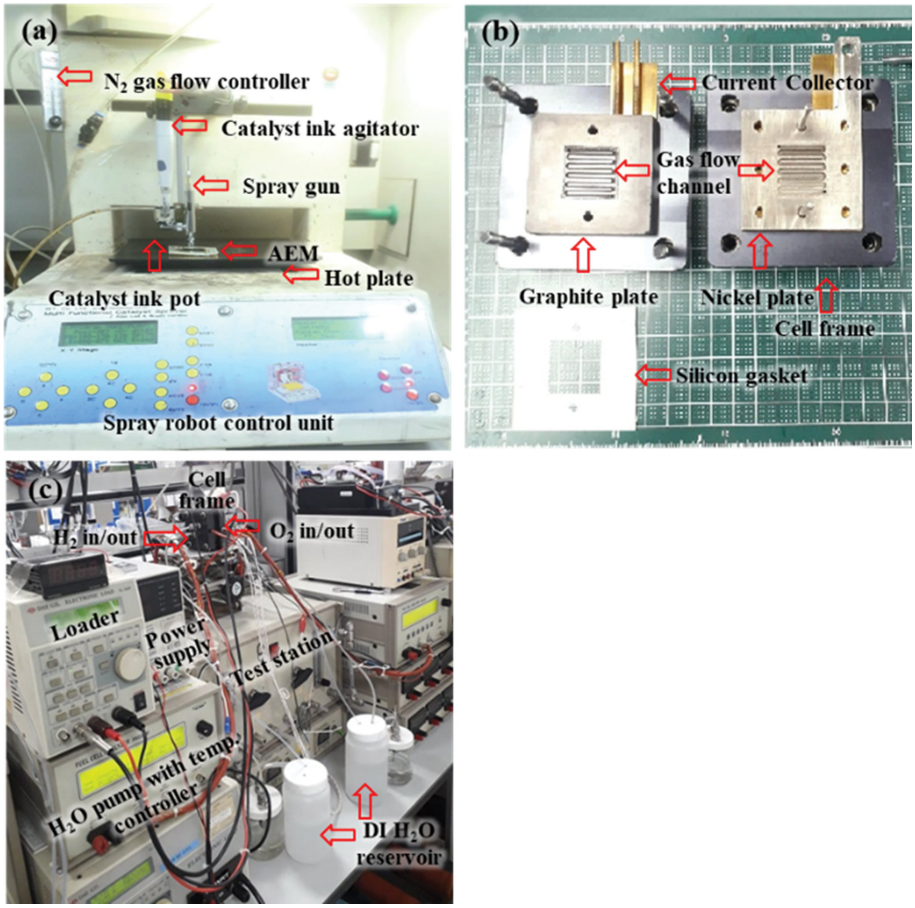

Fig. 2. Photograph of AEM-URFC fabrication and performance investigation, (a) CCM preparation, and (b) cell components, and (c) test station.

RESULTS AND DISCUSSION

The FAA-3 ionomer is a hydroxide ion (OH^-) conductor that provides an ionic pathway from the membrane to the catalyst layers. Low ionomer loading is insufficient to smooth conduct ions (OH^-) in the catalyst layer, but excessively high ionomer loading can block the active site of catalyst layers and the diffusion of gas, leading to a decrease in cell performance [13]. Fig. 3 reveals the representative SEM images of the prepared MEAs with 10 to 40 wt% ionomer contents. It can be detected that the agglomerates in the catalyst layers increase with increased ionomer content. More specifically, the MEA with 40 wt% ionomer content, the Pt/C catalysts are extremely isolated and the pores on the surface are severely blocked, which will hinder the electron and mass transport (water and gases), and thus demised both active area and catalyst use [14, 15]. Lower ionomer (10-20 wt%) content provide inadequate ionic conduction (OH^- ions) path, and excessive ionomer content may cover the active site of the catalysts. The catalyst layer's morphology, in terms of secondary pore formation, is also affected by the ionomer content [16,17]. As the ionomer content increased from 10 to 30 wt%, larger secondary pores were formed, but for 40 wt% ionomer content pores were blocked due to excessive ionomer (Fig. 3(c)). By contrast, the AEM-URFC performance for higher ionomer content of 40 wt% was worse than that for ionomer content of 30 wt%. Fig. 4 shows the ionomer content effect on the AEM-URFC performance. The cell performance increases when the ionomer content increases from 10 to 30 wt% and then decreases. As shown in Fig. 4(a), the cell performance of the four MEAs in WE mode was nearly similar. But in FC mode, at the high current density region, increased ionomer content resulted in increased cell performance [18]. The MEA containing ionomer content of 30 wt% exhibited higher performance than others. In FC mode, the cell performance increased with ionomer content from 10 to 30 wt% and then decreased. The MEA containing 30 wt% ionomer shows the highest current (200 mA/cm^2) and peak power density (100 mW/cm^2) at 0.5 V. In addition, open-circuit voltage (OCV) was observed at each ionomer content under the AEM-URFC operation (FC mode). The OCV increased from 1.0 V to 1.06 V for 10 wt% to 20 wt% and highest OCV value (1.08 V) for 30 wt% ionomer content. Above 30 wt% ionomer content, i.e., 40 wt% (1.045 V) OCV value decreased by about 35.0 mV. These results suggested that MEA's ionomer content greatly affects the AEM-URFC's cell performance. The diminished OCV in MEA containing 40 wt% of ionomer content is the indication of the decreased catalytic activity in the catalyst layers. Fig. 4(c)-(d) provides the in situ electrochemical impedance spectra (EIS) evaluated at 0.8 V. It is observed that the high-frequency resistance related to the ohmic resistance increases in a similar order of 10 wt%>40 wt%>20 wt%>30 wt%.

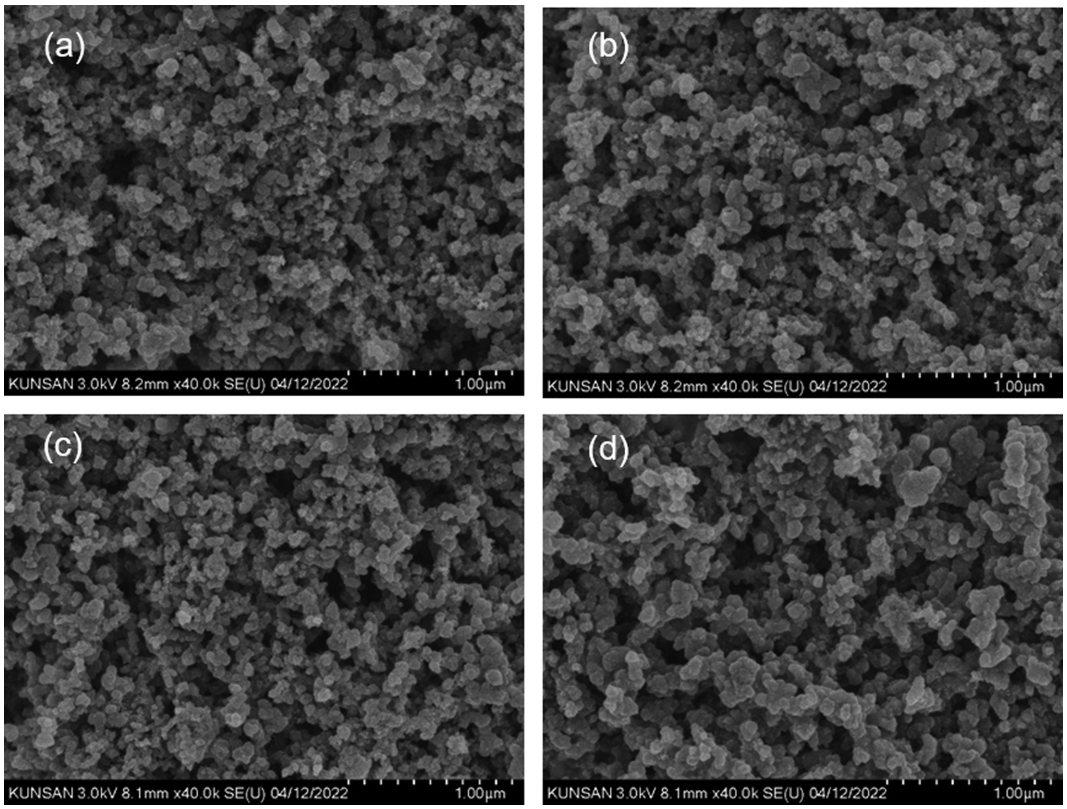

Fig. 3. SEM images of surface morphology of the CCMs at different ionomer content, including (a) 10 wt%, (b) 20 wt%, (c) 30 wt%, and (d) 40 wt% respectively.

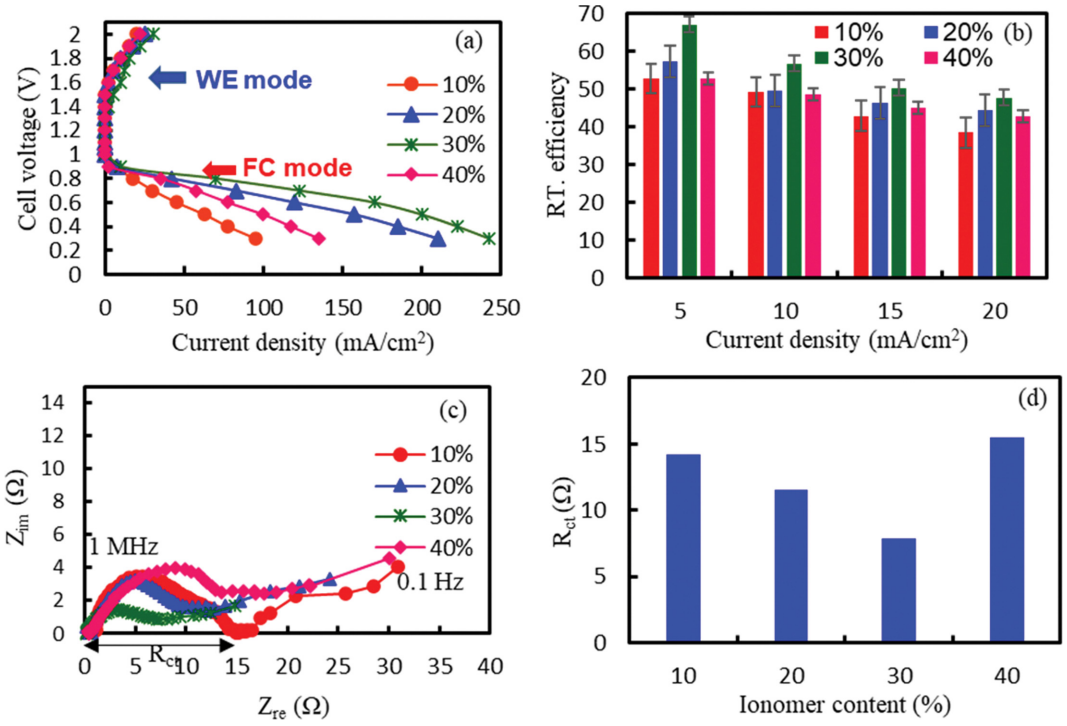

Fig. 4. Effect of ionomer content on the cell performance of AEM-URFC, (a) current density vs. cell voltage, (b) round trip efficiency at 20 mA/cm^2, (c) in-situ electrochemical impedance spectra (0.1 Hz to 1 MHz), and (d) charge transfer resistance at 0.8 V of single cell with different ionomer content. The MEAs were prepared with different FAA-3 ionomer content and Pt/C (2.00 mg/cm^2) as catalysts on both electrode (BHE & BOE) sides. The cell temperature was maintained at 50 °C.

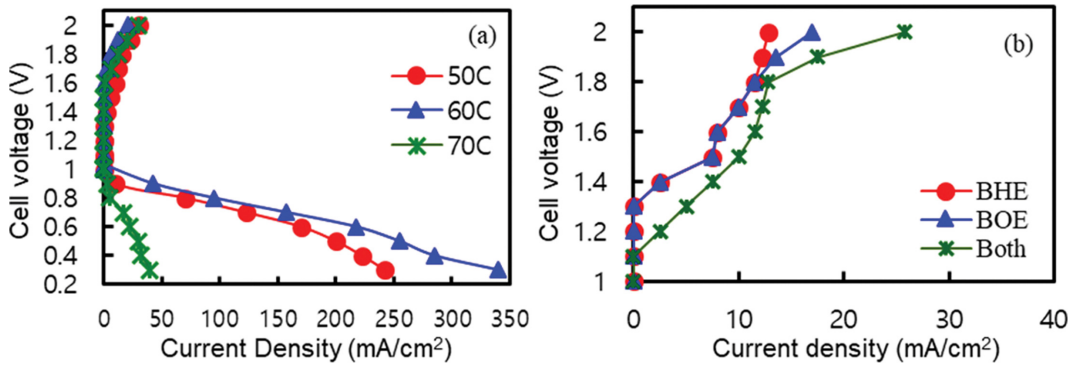

Fig. 5. Cell performance of AEM-URFC for different cell temperatures (a), and water feeding side (b). The MEAs were prepared with Pt/C (2.0 mg/cm^2) and 30 wt% FAA-3 ionomer.

On the other hand, the mass diffusion restriction inside the MEA can produce a double semicircle. These two arcs for the fuel cell system are specified as medium and low-frequency characteristics. The medium frequency characteristics represent the charge transfer resistance of the electrode reaction, and the low-frequency characteristic reveals the reactant mass transport resistance [19]. From EIS spectra, 30 wt% ionomer containing MEA achieves the lowest arcs both in the intermediate-frequency and low-frequency regions in the prepared MEAs, indicating the increased catalytic activity and reduced mass transport losses due to the enhanced triple phase boundaries (TPBs) and electrode microstructure. The RT efficiency of the four MEAs with different ionomer content (10, 20, 30, and 40 wt%) at 20.0 mA/cm^2 was 38.85%, 44.44%, 47.74%, and 42.99%, respectively (Fig. 4(b)). Thus, the RT efficiency also showed the highest value of 47.74% at 30 wt% ionomer content, which means 30 wt% of ionomer content was optimum for both WE and FC modes. The ionomer content above 30 wt% may block the micro and mesopores in the catalyst layers, which results in a decreased AEM-URFC cell performance [20-22].

Fig. 5 shows the effect of temperature on the cell performance of AEM-URFC. The cells were operated between 50 and 70 °C because at very high cell temperature AEM may be degraded. In FC mode, the cell performance was enhanced with increasing cell temperature from 50 to 60 °C due to the increased reaction kinetics of the reacting gases. The hydration of the membrane also plays a significant role in cell performance. Thus, the water content in the membrane increases with increasing temperature [23]. The cell at 50 °C has a low current (200.0 mA/cm^2 at 0.5 V) and peak power density (100.0 mA/cm^2) due to the low reaction kinetics. The cell shows improved performance at 60 °C and it has 255.0 mA/cm^2 of current density at 0.5 V and 48.3% RT efficiency at 20.0 mA/cm^2. At 70 °C, the FC performance continuously decreased, while the WE performance was not changed much. The higher temperature helps to raise the ionic conductivity with the increase of catalytic activity of the electro-catalyst [14,29]. At high temperatures, the charge transfer resistance and ohmic resistance also decreased. In WE mode, the cell performance increased with temperature. AEM-URFC's cell performance at 70 °C was increased by more than 40% over that at 50 °C, which was reported in the literature [24]. However, in this study, increasing cell temperature may damage the side chain of the functional group for ionic conduction. Water feeding to the BHE/BOE, or both electrodes were investigated in WE operation. The WE performance with different water supply modes is shown in Fig. 5(b). The water-feeding mode toward both electrodes in WE mode worked better than the water-feeding mode toward BHE or BOE. The hydroxide ion transfer in the AEM is generally done by the Grotthuss mechanism as in water. In the Grotthuss mechanism, hydroxide ions are dispersed via hydrogen-bonded water molecules [25,26]. Thus, ion transmission occurs along with the water in the membrane and the ionic conductivity of the electrolyte membrane is a significant function of the water content. Since water is essential for the hydroxide ions (OH^- ions) transport from the BHE side to the BOE side and around the TPBs, it would be good if the water was straightforwardly fed to that side where it would consume, i.e., the BOE catalyst layers [27]. Whereas in BHE water feeding mode, there is no adequate amount of water provided to the BOE side [28]. In BHE water feeding mode, the cell showed maximum current density at 2.0 V is 12.75 mA/cm^2. That is because the water flows direction in BHE water feeding mode as opposed to that of OH^- ions transfer, resulting in the inadequate water supply. The performance of the dual water feeding mode (2.25 ml/min) is slightly better than that of the single (BOE and BHE) feeding modes (2.25 ml/min) due to adequate water supply for electrolysis. In dual feeding mode, the cell shows maximum current density at 2.0 V is 25.7 mA/cm^2, which is twice of BHE mode. Therefore, both side water feeding (BHE and BOE feeding) is the optimal water feeding method. The cross-sectional SEM of MEAs for different catalyst loading is shown in Fig. 6. The surface morphology of the MEAs for the different catalyst loading is almost the same as the ionomer loading (Fig. 3). With increasing catalyst loading, micro and macropores are decreased and the catalyst thickness is increased. (Fig. 6 and Fig. 8(c)). The effect of catalyst (Pt/C) loading on the cell performance of AEM-URFC fabricated with FAA-3 ionomer (30 wt%) and membranes is shown in Fig. 7(a). The cell performance of AEM-URFC increased with increasing catalyst loading up to a maximum value as an effect of the improved catalytic activity and reduced resistances (ohmic and charge transfer resistance) [29]. Ohmic and charge transfer resistances are increased as same order of 1.0 mg/cm^2>1.50 mg^2>0.50 mg/cm^2>2.5 mg/cm^2>2.0 mg/cm^2. Mass transport resistance increases above 2.0 mg/cm^2 catalyst loading due to thick layers. Diffusion resistance is also equal to the

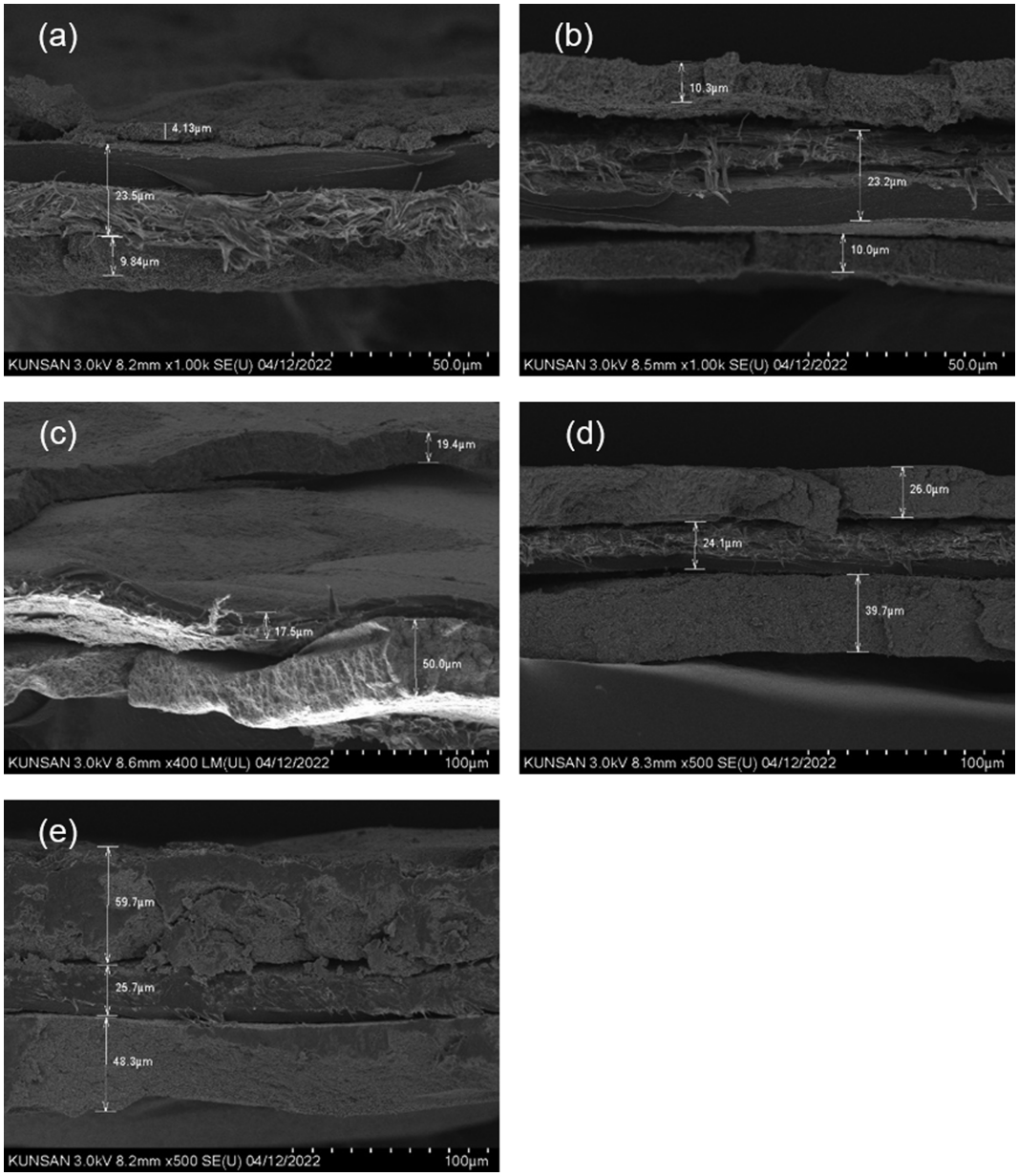

Fig. 6. Cross-sectional SEM images of the prepared CCMs at different catalyst loading, including (a) 0.50 mg/cm^2, (b) 1.00 mg/cm^2, (c) 1.50 mg/cm^2, (d) 2.00 mg/cm^2, and (e) 2.50 mg/cm^2 respectively.

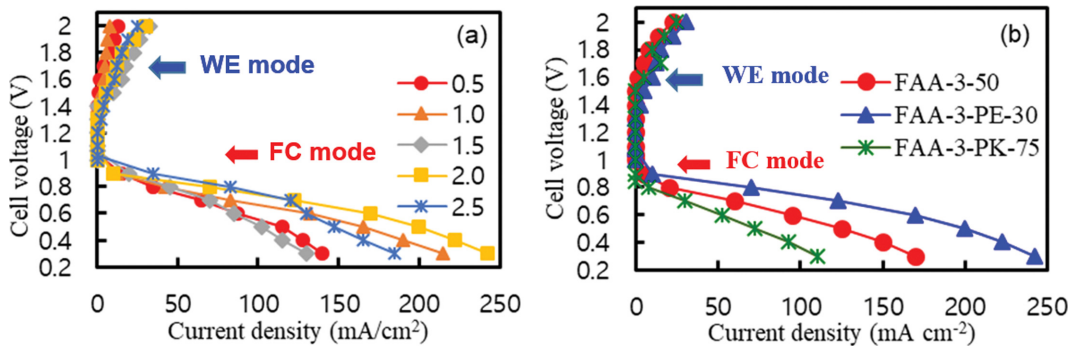

Fig. 7. Cell performance of AEM-URFC for different catalyst loading (a), and AEM types (b). The MEAs were prepared with Pt/C as a catalyst and 30 wt% FAA-3 ionomer. The cell temperature was maintained at 50 °C.

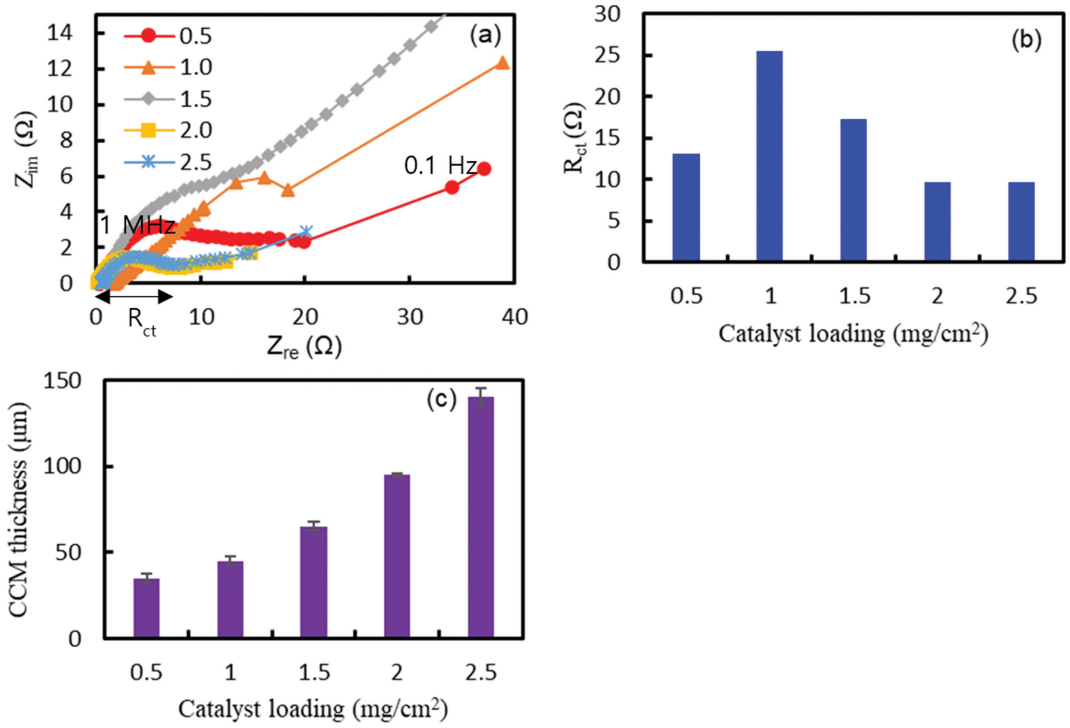

Fig. 8. In-situ electrochemical impedance spectra at frequency range of 0.1 Hz to 1 MHz (0.8 V) (a), charge transfer resistance (b), and thickness (c) of the prepared CCMs for different catalyst loading.

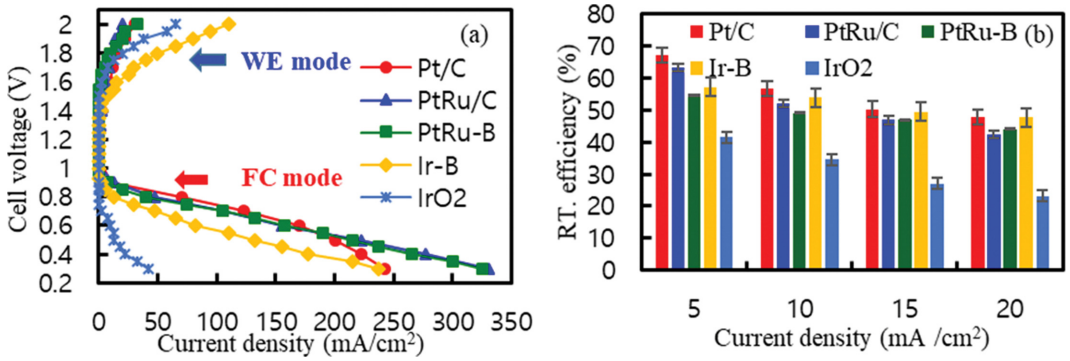

Fig. 9. Cell performance of AEM-URFC for different BOE catalysts. (a) Current density vs. cell voltage, and (b) round-trip efficiency at 20 mA/cm^2. The MEAs were prepared with Pt/C (2.0 mg/cm^2) at BHE and different BOE catalysts (2.0 mg/cm^2).

mass transport resistance inside the MEAs (Fig. 8(a)-(b)). Further increased above the maximum loading decreased the cell performance. Because increased catalyst content forms very thicker layers which may hinder the gas transport, which affects the cell performance. Here we display an incremental increase of catalyst content from 0.5 to 2.5 mg/cm^2. While other researchers generally use higher catalyst loading as 1-4 mg/cm^2 [30,31]. It can be observed that an MEA making with 2.0 mg/cm^2 of Pt loading performs the best cell performance reaching 200.0 and 30.5 mA/cm^2 of the current density at 0.5 and 2.0 V, respectively. This MEA shows maximum peak power density was 100 mW/cm^2 at 0.5 V. The OCV of these cells steadily improved to the peak of 1.040 V at Pt loading of 0.5 mg/cm^2 to 1.06 V (1.0 mg/cm^2), 1.064 (1.50 mg/cm^2) and the peak of 1.08 V for 2.0 mg/cm^2 loading. After dropping by 47.0 mV (1.033 V) at Pt loading of 2.5 mg/cm^2. This indicates that the reactant gas transport was hindered steadily due to the thicker catalyst layer of the increasing catalyst loading; however, high loading (above 2.0 mg/cm^2) forms thicker catalyst layers that hinder the reactant gas transportation at the boundary of the catalyst layer and AEM. Higher ohmic and charge transfer resistances are also crucial factors in voltage drop. Although 2.5 mg/cm^2 of Pt loaded MEA shows better performance in WE mode, it has poor cell performance in FC mode, due to the thicker catalyst layer formation (Fig. 6 and Fig. 8(c)). High cell performance with RT efficiency of MEA with 2.0 mg/cm^2 of Pt loading has the additional preference for use in AEM-URFC. Anion exchange membrane (AEM) is one of the most important key components of the AEM-URFC. AEM has a direct influence on the cell performance of AEM-URFC. For

this reason, we investigated the cell performance of commercially accessible anion exchange membranes, such as Fumasep FAA-3-50, FAA-3-PE-30, and FAA-3-PK-75 manufactured by Fumatech GmbH. The other electrode parameters were the same as in the previous study. In Fig. 7(b), the OCV for the FAA-3-50, FAA-3-PE-30, and FAA-3-Pk-75 was 1.04, 1.08 and 0.847 V, respectively. At the low current density region (activation region) in FC mode, FAA-3-50 shows better performance than the FAA-3-PK-75 and the same as FAA-3-PE-30. But at a high current density region, the FAA-3-PE-30 shows better performance than FAA-3-50 and FAA-3-PK-75 [32]. However, we could not find a distinguishable difference in the WE performance of the three AEMs. The RT efficiency of the AEMs was 40.82 (FAA-3-50), 47.65 (FAA-3-PE-30), and 38.49% (FAA-3-PK-75), respectively. The physical and chemical properties of AEMs are listed in Table 1. FAA-3-PE-30 has relatively high ion exchange capacity and low area resistance, compared with FAA-3-50 and PK-75. Also, FAA-3-PE-30 is the thinnest film among the three AEMs and has mechanical strength because it is reinforced by polyethylene fiber. Based on these properties, AEM-URFC with FAA-3-PE-30 showed the highest cell performance among them.

The BOE catalyst plays a significant role in the cell performance of AEM-URFC. The BOE catalyst should act as the catalyst for the ORR and OER simultaneously. We investigated the AEM-URFC cell performance with different BOE catalysts (Fig. 9). The reaction rate of BHE is relatively fast, while ORR is the responsible step for the whole progression. The BOE catalyst has more influence on the performance than the BHE catalyst. The BOE used in this study comprised Pt- and Ir-based catalysts. Carbon-supported Pt catalyst has been widely used for ORR in fuel cells. The carbon support recommends a large surface area and smaller Pt nanoparticles. It is also responsible for the secondary pore growth that superior mass (gas) passage, resulting in enhanced cell performance [33,34]. When the catalyst at BOE, Pt/C (40 wt%) changed with PtRu/C (60 wt%), the current density at 0.5 V (FC mode) was enhanced by a factor of ~1.40, which was attributed to the increased number of active sites from Ru particles [35]. But due to the carbon support, it is rusted easily at high cell voltage (WE mode). To resolve these problems, PtRu black (PtRu-B) was used. PtRu-B shows similar in FC mode but slightly higher cell performance in WE mode than PtRu/C. To enhance performance for WE, the Ir-based materials including Ir black (Ir-B) and IrO_2 were applied to the BOE catalyst. Since Ir-B has superior stability to IrO_2 in alkaline media [36]. From Fig. 9, Ir-B and IrO_2 considerably affected the WE performance, which shows 3.4 and 2.0 times higher current than that for PtRu-B at 2.0 V, respectively. However, those showed lower FC performance than PtRu-based catalysts. The MEA with Ir-B in BOE shows 220.0 and 110.0 mA/cm^2 at 0.3 and 2.0 V, respectively. And the AEM-URFC containing Ir-B in BOE catalyst exhibited RT efficiency of 47.81% at the current density of 20.0 mA/cm^2, which is comparable, or superior, to the report in the literature [37]. The cell performance of AEM-URFC with different catalysts at BOE is

Table 1. Physical and chemical profile of the AEMs (supplied from Fumatech GmbH)

AEM	Thickness (μm)	Ion exchange capacity (in Cl^- form) (meq/g)	Area resistance (in Cl^- form) (Ω/cm^2)	H_2O uptake (at 25 °C)	Reinforcement
FAA-3-50	45-55	1.60-2.10	0.60-1.50	10-25 wt%	None
FAA-3-PE-30	20-30	1.40-1.60	0.80-1.30	15-20 wt%	PE[a]
FAA-3-PK-75	70-80	1.20-1.40	1.20-2.00	10-20 wt%	PK[b]

[a]PE: Polyethylene, [b]PK: Polyether ketone

Table 2. Summary of AEM-URFCs cell performance in FC and WE modes compared with results reported in the literature

BHE (mg/cm^2)		BOE (mg/cm^2)		Membrane	Temp. (°C)	Current (mA/cm^2)		RT Eff.[a] (%)	Ref.
						FC mode at 0.5 V	WE mode at 2.0 V		
Pt/C	2.0	Pt/C	2.0	FAA-3-PE-30	50	200.0	18.3	47.6	This work
Pt/C	2.0	Pt/C	2.0	FAA-3-PE-30	60	255.0	20.3	48.3	
Pt/C	2.0	PtRu/C	2.0	FAA-3-PE-30	50	222.5	20.0	42.5	
Pt/C	2.0	PtRu-B	2.0	FAA-3-PE-30	50	215.0	32.5	44.1	
Pt/C	2.0	IrO_2	2.0	FAA-3-PE-30	50	12.5	65.0	23.1	
Pt/C	2.0	Ir-B	2.0	FAA-3-PE-30	50	132.5	110.0	47.8	
Pt/C	0.5	MnO_x-SS	0.5	FAA-3-PK-130	55	48.0	58.0 (1.7 V)	45.0	[38]
Pt/C	0.5	Pt/C	0.5	A-201 (Tokuyama)	50	120.0	25.0	50.0	[11]
Ni/C	6.0	MnO_x/GC : Ni/C	4.0	FAA-3-20	65	22.0	17.5 (1.85 V)	40.0	[39]
Pt/C	1.0	$Cu_xMn_{0.9-x}Co_{2.1}O_4$	3.0	Home made	40	130.0	180.0	44.51	[40]
Pt/C	3.3	$NiFeO_x$/CoNy-C	6.6	TK-PEEK	25	275.0	120.0[b] (1.6 V)	51.5	[41]
Pt/C	0.80	IrO_2/C	0.80	TK-PEEK	25	85.0	125.0[b] (1.65 V)	44.76	[42]

[a]Round trip efficiency at 20 mA/cm^2 with DI water feeding, [b]3 M KOH feeding.

summarized compared with others reported in the literature in Table 2. Our results of AEM-URFC running without any KOH solution feeding to electrodes are comparable to those reported in the literature.

CONCLUSIONS

The effects of electrode parameters and operating conditions were investigated on the cell performance of AEM-URFC. The ionomer content in electrode, cell temperature, and water feeding type highly affected the cell performance of AEM-URFC. We found optimum ionomer content (30%) in the catalytic layer of the electrode and the best water-feeding type supplied to both electrodes, BHE and BOE. Thinner AEM gave better cell performance in FC mode but was similar in WE mode. Pt-based catalysts for BOE showed better cell performance for FC mode but relatively low for WE mode. When those were changed to Ir-based ones for BOE, the current reached 110.0 mA/cm^2 at 2.0 V in WE mode, which was 2.0-3.4 times higher than Pt-based catalysts, but they were not highly active in FC mode, which was 60% of the current at 0.5 V for the latter. Our results of AEM-URFC running with pure water feeding to the electrode are comparable with those reported in the literature.

ACKNOWLEDGEMENT

This work was supported by the Technology Innovation Program of Korea Evaluation Institute of Industrial Technology (KEIT) grant funded By the Ministry of Trade, Industry & Energy (MOTIE, Korea) (No. 20002425) and the National Research Foundation of Korea (NRF) grant funded by the Korea government (MSIT) (No. 2021R1I1A3057906). Also, this research was supported by Gunsan City, Korea, under the Human Resources Program for the EV industrial cluster.

STATEMENTS AND DECLARATIONS

Conflict of Interest

The authors declare that they have no known competing financial interests or personal relationships that could have appeared to influence the work reported in this paper.

The authors declare the following financial interests/personal relationships which may be considered as potential competing interests.

REFERENCES

1. A. Sarapuu, E. Kibena-Põldsepp, M. Borgheib and K. Tammeveski, *J. Mater. Chem. A*, **6**, 776 (2018).
2. S.-D. Yim, W.-Y. Lee, Y.-G. Yoon, Y.-J. Sohn, G.-G. Park, T.-H. Yang and C.-S. Kim, *J. Electrochim. Acta*, **50**, 713 (2004).
3. J. Pettersson, B. Ramsey and D. Harrison, *J. Power Sources*, **157**, 28 (2006).
4. H. P. Dhar, *J. Appl. Electrochem*., **23**, 32 (1993).
5. Y. Wang, D. Y. C. Leung, J. Xuan and H. Wang, *Renew. Sustain. Energ. Rev.*, **65**, 961 (2016).
6. R. Omrani and B. Shabani, *Int. J. Hydrog. Energy*, **44**, 3834 (2019).
7. X. Wu and K. Scott, *J. Mater. Chem*., **21**, 12344 (2011).
8. L. Xiao, S. Zhang, J. Pan, C. Yang, M. He, L. Zhuang and J. Lu, *Energy Environ. Sci*., **5**, 7869 (2012).
9. S. Gottesfeld, D. R. Dekel, M. Page, C. Bae, Y. Yan, P. Zelenay and Y. S. Kim, *J. Power Sources*, **375**, 170 (2018).
10. S. Lu, J. Pan, A. Huang, L. Zhuang and J. Lu, *Proc. Natl. Acad. Sci. U.S.A*., **105**, 20611 (2008).
11. S. Dresp, F. Luo, R. Schmack, S. Kühl, M. Gliech and P. Strasser, *Energy Environ. Sci*., **9**, 2020 (2016).
12. X. Wu and K. Scott, *J. Power Sources*, **214**, 124 (2012).
13. G. Li and P. G. Pickup, *J. Electrochem. Soc*., **150**, C745 (2003).
14. M. Mamlouk, K. Scott, J. A. Horsfall and C. Williams, *Int. J. Hydrogen Energ*., **36**, 7191 (2011).
15. D. Yang, H. Yu, G. Li, Y. Zhao, Y. Liu, C. Zhang, W. Song and Z. Shao, *J. Power Sources*, **267**, 39 (2014).
16. S. J. Paddison and K. S. Promislow, *Device and materials in PEM fuel cells*, Springer Science & Business Media, New York (2008).
17. M. Ünlü, J. Zhou, I. Anestis-Richard, H. Kim and P. A. Kohl, *J. Electrochim. Acta*, **56**, 4439 (2011).
18. M. Carmo, G. Doubek, R. C. Sekol, M. Linardi and A. D. Taylor, *J. Power Sources*, **230**, 169 (2013).
19. R. V. John, C. T. S. Robert, L. W. Graham and C. Yanling, *J. Phys. Chem. B*, **110**(42), 21041 (2006).
20. J. E. Park, S. Y. Kang, S. H. Oh, J. K. Kim, M. S. Lim, C. Y. Ahn, Y. H. Cho and Y. E. Sung, *Electrochim. Acta*, **295**, 99 (2019).
21. P. Gode, F. Jaouen, G. Lindbergh, A. Lundblad and G. Sundholm, *Electrochim. Acta*, **48**, 4175 (2003).
22. M. K. Cho, H.-Y. Park, S. Choe, S. J. Yoo, J. Y. Kim, H.-J. Kim, D. Henkensmeier, S. Y. Lee, Y.-E. Sung, H. S. Park and J. H. Jang, *J. Power Sources*, **347**, 283 (2017).
23. Y. S. Li, T. S. Zhao and W. W. Yang, *Int. J. Hydrogen Energ*., **35**, 5656 (2010).
24. S. H. Ahn, B. S. Lee, I. Choi, S. J. Yoo, H. J. Kim, E. A. Cho, D. Henkensmeier, S. W. Nam, S. K. Kim and J. H. Jang, *J. Appl. Cat. B: Environ*., **154-155**, 197 (2014).
25. C. Chen, Y.-L. S. Tse, G. E. Lindberg, C. Knight and G. A. Voth, *J. Am. Chem. Soc*., **138**, 991 (2016).
26. S. Maurya, S.-H. Shin, Y. Kim and S.-H. Moon, *J. RSC Adv*., **5**, 37206 (2015).
27. D. Li, E. J. Park, W. Zhu, Q. Shi, Y. Zhou, H. Tian, Y. Lin, A. Sherov, B. Zulevi, E. D. Baca, C. Fujimoto, H. T. Chung and Y. S. Kim, *J. Nat. Energy*, **5**, 378 (2020).
28. M. K. Cho, H.-Y. Park, H. J. Lee, H.-J. Kim, A. Lim, D. Henkensmeier, S. J. Yoo, J. Y. Kim, S. Y. Lee, H. S. Park and J. H. Jang, *J. Power Sources*, **382**, 22 (2018).
29. D. Yang, H. Yu, G. Li, W. Song, Y. Liu and Z. Shao, *Chin. J. Catal*., **35**, 1091 (2014).
30. Y. Zhang, C. Wang, N. Wan and Z. Mao, *Int. J. Hydrogen Energ*., **32**, 400 (2007).
31. S. D. Yim, G. G. Park, Y. J. Sohn, W. Y. Lee, Y. G. Yoon, T. H. Yang, S. Um, S. P. Yu and C. S. Kim, *Int. J. Hydrogen Energ*., **30**, 1345 (2005).
32. M. J. Jang, M. S. Won, K. H. Lee and S. M. Choi, *J. Korean Inst. Surf. Eng*., **49**, 159 (2016).
33. E. Antolini, *J. Appl. Catal. B: Environ*., **88**, 1 (2009).

34. Z. A. C. Ramli and S. K. Kamarudin, *J. Nanoscale Res. Lett.*, **13**, 410 (2018).
35. P. Gayen, S. Saha, X. Liu, K. Sharma and V. K. Ramani, *PNAS*, **118**(40), e2107205118 (2021).
36. S. Cherevko, S. Geiger, O. Kasian, N. Kulyk, J.-P. Grote, A. Savan, B. R. Shrestha, S. Merzlikin, B. Breitbach, A. Luding and K. J. J. Mayrhofer, *J. Catal. Today*, **262**, 170 (2016).
37. X. Zhuo, S. Sui and J. Zhang, *Int. J. Hydrogen Energ.*, **38**, 4792 (2013).
38. J. W. D. Ng, M. Tang and T. F. Jaramillo, *J. Energy Environ. Sci.*, **7**, 2017 (2014).
39. J. W. D. Ng, Y. Gorlin, T. Hatsukade and T. F. Jaramillo, *Adv. Energy Mater.*, **3**, 1545 (2013).
40. X. Wu and K. Scott, *J. Power Sources*, **206**, 14 (2012).
41. H. Zhong, R. Tian, X. Gong, D. Li, P. Tang, N. Alonso-Vante and Y. Feng, *J. Power Sources*, **361**, 21 (2017).
42. C. A. Campos-Roldán, H. Zhong, S. M. Unni, R. de G. González-Huerta, Y. Feng and N. Alonso-Vante, *ACS Appl. Energy Mater.*, **3**(8), 7397 (2020).